

Scanning near-field optical microscopy measurements and simulations of regularly arranged silver nanoparticles

M Song^{1,2}, P Fumagalli¹ and M Schmid^{1,2,3,*} 

¹Institut für Experimentalphysik, Freie Universität Berlin, D-14195 Berlin, Germany

²Nanooptische Konzepte für die PV, Helmholtz-Zentrum Berlin für Materialien und Energie GmbH, D-14109 Berlin, Germany

³Faculty of Physics and CENIDE, University of Duisburg-Essen, Forsthausweg 2, D-47057 Duisburg, Germany

E-mail: martina.schmid@uni-due.de

Received 30 August 2023, revised 19 October 2023

Accepted for publication 6 November 2023

Published 22 November 2023



CrossMark

Abstract


Silver nanoparticles on a glass substrate are experimentally investigated by aperture scanning near-field optical microscopy (a-SNOM). To understand the experimental results, finite-element-method simulations are performed building a theoretical model of the a-SNOM geometry. We systematically vary parameters like aperture size, aluminum-coating thickness, tip cone angle, and tip-surface distance and discuss their influence on the near-field enhancement. All these investigations are performed comparatively for constant-height and constant-gap scanning modes. In the end, we establish a reliable and stable optical model for simulating a-SNOM measurements, which is capable of reproducing trends observed in experimental data.

Keywords: SNOM, silver nanoparticle, FEM simulation, plasmonic enhancement

1. Introduction

Scanning near-field optical microscopy (SNOM or NSOM) has made a remarkable contribution to nanoscience as it offers subwavelength resolution imaging and spectroscopy by combining scanning-probe technology with optical microscopy. It merges the advantages of being a non-destructive, vacuum-free, and low-cost method that can be applied to various sample types and is relatively easy to operate. The technology provides a powerful tool to study e.g. surface plasmon polaritons (SPP) [1–6] or localized surface plasmons (LSP) [7–11] with high spatial resolution and has hence found application in different research fields like physics [1–8, 11–13], chemistry [9, 14], and life science [15, 16].

* Author to whom any correspondence should be addressed.

 Original content from this work may be used under the terms of the [Creative Commons Attribution 4.0 licence](https://creativecommons.org/licenses/by/4.0/). Any further distribution of this work must maintain attribution to the author(s) and the title of the work, journal citation and DOI.

SNOM can be employed in scattering configuration (s-SNOM), where laser light scattering from a metal tip is exploited for near-field generation, or in aperture mode (a-SNOM), where a tip with a small opening is used. In the latter case, either the illumination or the detection may occur via the aperture tip, leading to the so-called illumination or collection mode, respectively. Thus, in illumination mode, the generation of localized near fields at the surface happens with an aperture tip, whilst the detection takes place in the far field, i.e. far away from the tip. In other words, the relevant light-matter interaction occurs in the near field at the sample surface, but the optical image is formed in the far field by detecting intensity changes at very large distances from the sample. Therefore, the need arises to investigate how the evanescent fields transform into propagating fields carrying near-field information about the sample.

For fundamentally understanding the mechanism of tip-sample interaction, versatile and at the same time accurate computational methods are required. However, there are various challenges involved due to the high complexity of the SNOM system including different length scales: the sample

features under investigation are usually nano- or microscopic, whilst they are adherent to a semi-infinite substrate that also influences the optical behavior. The tip is orders of magnitude larger than the nanostructures, yet the interaction is very subtle and strongly influenced by the nanoscopic features of the tip end as well as by the scanning process.

Starting from the 1990s, great efforts have been devoted to theoretically understanding image formation in near-field optical microscopy, see for example the two extensive review articles by Girard and Dereux [17] and Greffet and Carminati [18]. Besides, there is a later review focusing on imaging by s-SNOM and a-SNOM in collection mode (here called c-SNOM) [19]. In the last years, many papers have been published on SNOM measurements of plasmonic and photonic nanostructures and the comparison to numerically calculated field distributions of the same. An abundant summary is impossible, thus we just mention three examples, namely the investigation of Airy surface plasmons [20], and phase micro-Fresnel zone plates [21], (both employing a-SNOM in collection mode), as well as imaging random metal nanoparticle arrays using a-SNOM in illumination mode [22]. Regarding the theoretical investigation and simulation of SNOM measurements including the tip, the literature, however, is not as extensive. 1D/2D analytical simulations of s-SNOM configurations can e.g. be found in [23, 24]. An experimental and numerical study of a-SNOM in collection mode under consideration of the tip was performed using simulations in finite-difference time domain (FDTD) with an emphasis on variations of illumination wavelength and polarization [25]. As to a-SNOM in illumination mode, the mechanism of image formation was investigated for magnetic fields experimentally and numerically under consideration of the tip in FDTD simulations [26]. Recently, a dual tip SNOM was used to image with one tip the near-field emission pattern from the other one, and the experimental results were brought in line with numerical calculations based on the Bethe–Bouwkamp theory; interestingly, different tip geometries and coatings were considered [27].

Our focus is on the regularly used single-tip configuration of an a-SNOM in illumination mode, i.e. the illumination occurs through a small opening at the tip end and the detection takes place in the far field. Furthermore, we treat the tip in a multi-dimensional manner and extend the range of parameters considered in the simulations for the aperture size, the coating thickness, and the cone angle as well as the distance between tip and sample. For this purpose, we revert to numerical simulations employing the finite-element method (FEM). It allows a meshing that is highly adaptive to the respective geometry and a local solution of Maxwell's equations.

The software used is COMSOL Multiphysics and we apply it to describe experimental measurements of regularly arranged silver nanoparticles on a glass substrate. We consider various parameters describing the tip geometry like aperture size, cone angle, coating thickness, or tip shape. Furthermore, we study the tip-particle interaction by considering different scanning modes and sweeping the distance between the sample and the tip. The calculation results are

compared to the experimental measurements and finally, a numerical 2D model is established for describing the SNOM investigation of nanoparticles.

2. Experiment and simulation

2.1. Experimental configuration and measurements

The near-field of silver nanoparticles is investigated by experiment and used as a reference for the simulations. A sample of regularly arranged silver nanoparticles is produced by shadow nanosphere lithography using polystyrene spheres as a mask [28]. After the deposition of a 60 nm silver film on the close-packed polystyrene-sphere mask the spheres are dissolved. As a consequence, regular metal patches are left on the glass substrate at the original interstices. To form spherical nanoparticles, the sample is annealed at 300 °C for 20 min, resulting in silver nanoparticles with 140 ± 20 nm diameter.

Such samples of silver nanoparticles are measured with a custom-built a-SNOM in illumination mode. Whereas a classical atomic force microscope (AFM) exploits the forces emerging between the tip and the sample for profiling the surface topography, a SNOM additionally collects optical information, which in the case of a-SNOM results from illumination and/or detection through an opening in a fiber-based tip. In our case, a 532 nm CW laser is coupled into the aperture tip and illuminates the particles in the near field as shown in figure 1(a) (illumination mode). Figure 1(b) presents the topography of the silver nanoparticles obtained during the scanning probe measurement. Transmitted and reflected electric field intensities are simultaneously recorded while scanning across the particles and are shown in figures 1(c) and (d).

The transmission results reveal minimum intensity at the position of the nanoparticles and an enhanced field around them. This circumferential field enhancement is commonly observed for the interaction of unpolarized light with metal nanoparticles resulting in fundamental and higher order modes and can there be attributed to localized surface plasmon polaritons [29]. Another dip in transmission intensity is found at the center of the hexagonal ring formed by six particles, highlighting the interaction of immediately neighboring particles in between which high intensities are observed. On the other hand, the reflectivity shows enhancement on the top of the particles representing metallic reflection. A circular enhancement around the hexagonal unit cell formed by every six particles is also obvious in the reflectivity as shown in figure 1(d). A lower intensity signal together with more pronounced fine structures is typical for reflectivity measurements since the scattered light has to be detected under an angle where no shading from the tip occurs. Figures 1(e)–(g) show line profiles through two directly adjacent nanoparticles as extracted from the pictures in figures 1(b)–(d). The high and low-intensity areas are clearly visible as is the higher noise in the reflectivity measurement.

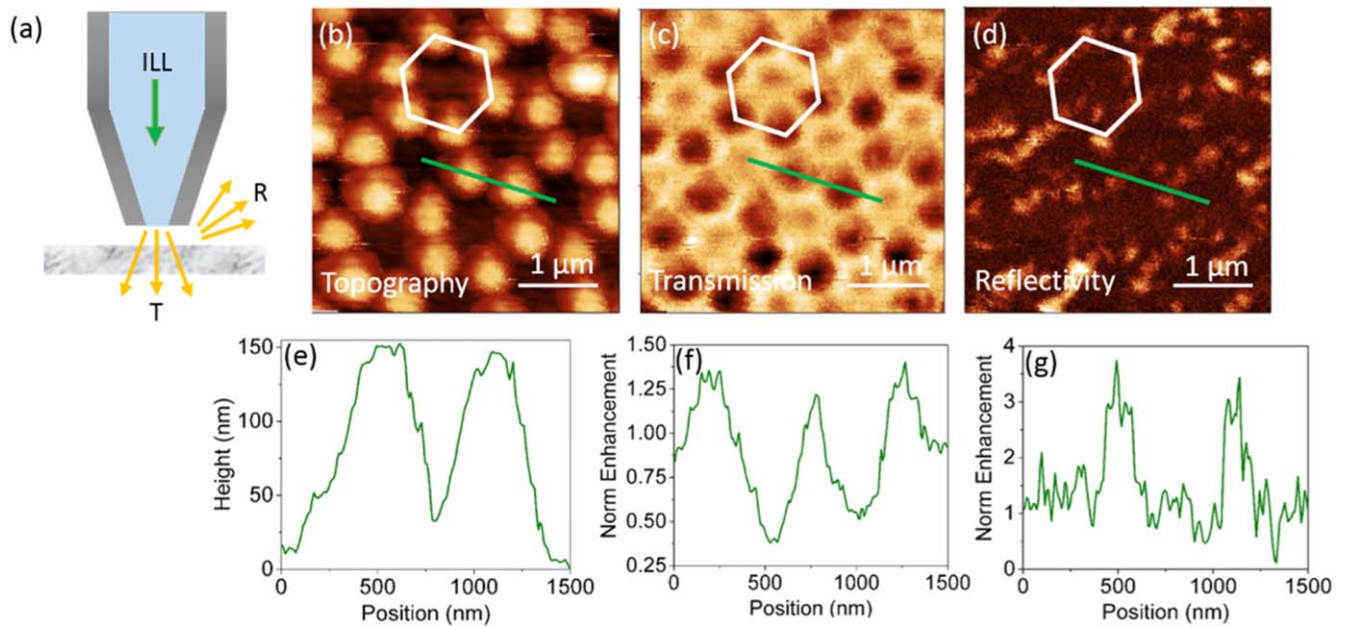


Figure 1. Results of aperture SNOM measurement in illumination mode: (a) sketch of the tip-matter interaction, (b) topography, (c) transmitted intensity (transmission), (d) reflected intensity (reflectivity), and (e)–(g) line scans from (b)–(d) along the indicated green lines.

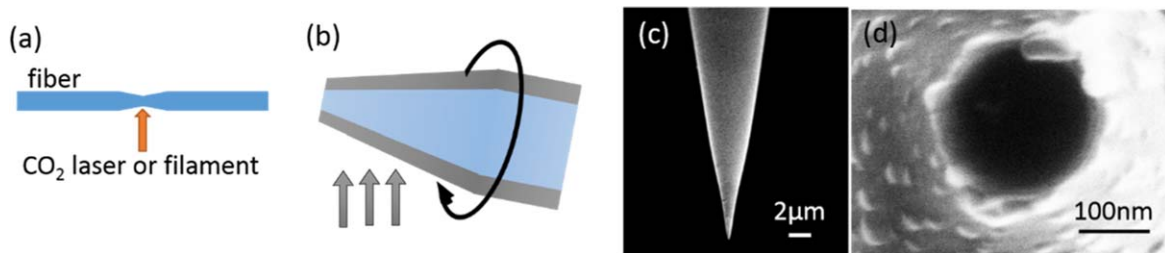


Figure 2. Fiber-based aperture-tip fabrication: (a) tapered fiber prepared by heating and pulling, (b) evaporation geometry of the aluminum-coating process: evaporation takes place under an angle slightly from behind while the tip is rotating, (c) and (d) SEM images of aluminum-coated aperture tips prepared by pulling.

For an improved understanding of the experimental results, a numerical simulation model is required. However, SNOM is a very complex system with various parameters to be considered. The most critical part is the aperture tip. In this work, a commercial aperture tip (LovaLite, type E50, HPSC10 multimode fiber, Al coated, 100 nm aperture) is used which was fabricated from a fiber in two main steps as shown in figure 2. First, a transparent taper with a sharp apex is created by heating with a CO₂ laser and pulling [figure 2(a)]. Second, an entirely opaque aluminum film is coated on the cone walls to form a transmissive aperture at the apex only [figure 2(b)]. The aluminum coating is conducted under an angle while rotating the tip, to form an opening at the tip end. This fiber-based tip has a sharp end with an opening of around 300 nm in diameter as shown in the scanning electron microscopy (SEM) images figures 2(c) and (d).

According to the fabrication process, several parameters have to be considered. First of all, the tapering and pulling process introduces the variables angle of the tip end and size of its opening. The coating thickness can be set to a well-defined value. Due to the coating angle and the tip rotation, the thickness of the coating at the tip end, however, is not well

defined, thus creating another variable. Additionally, from SEM images of the fabricated tip, it is clear that the very end of the tip is neither smooth nor has a sharp and clean edge. Tiny grains are present at the side of the tip and at the opening edge. They should be considered as a parameter of tip roughness or specific shape in the simulation. Following the observation of these variables, three main parameters are included in the tip model as shown in figure 3(a): angle of the tapered end (cone angle), size of the aperture (opening), and thickness of the aluminum coating (coating). Considering the roughness and attached tiny grains at the very end of the tip, later on, different shapes of the tip are considered in addition. Furthermore, the parameter gap describes the shortest distance between the tip end and the nanoparticle surface.

With a shear-force feedback control system, SNOM can be operated in two widely used modes of scanning the tip across the object as shown in figures 3(b) and (c). In constant-gap mode, the SNOM tip is held at a constant distance (equals gap) to the sample surface, which simultaneously provides the topography information. However, the tip height, changing with the sample surface, results in a coupling between the optical near-field signal and the topography. In contrast,

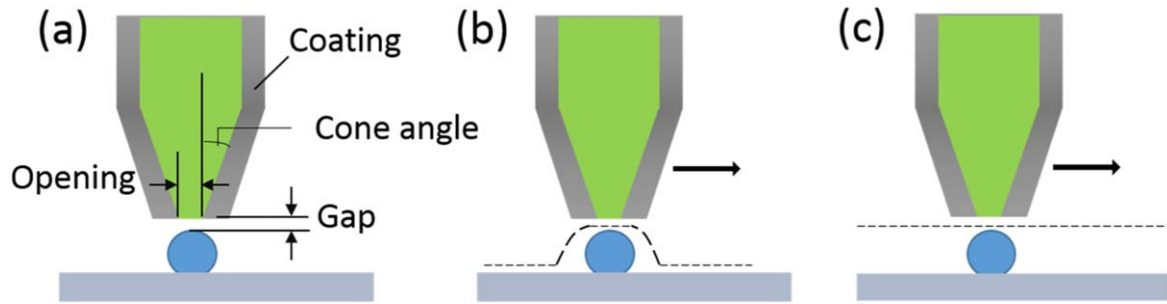


Figure 3. (a) Critical parameters for a simplified 2D model of an a-SNOM tip; (b) constant-gap scanning mode; (c) constant-height scanning mode.

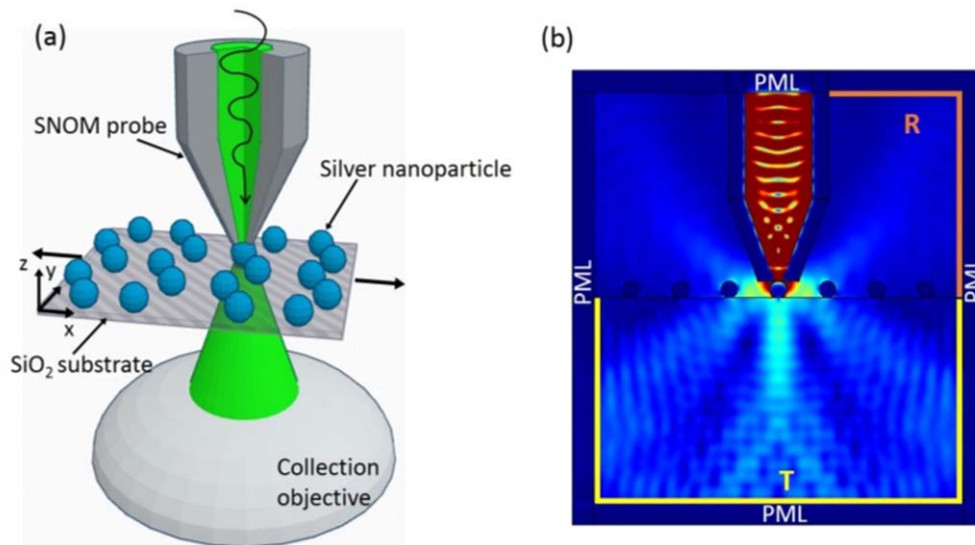


Figure 4. (a) Schematic of a typical a-SNOM geometry in illumination mode: near-field excitation of the silver nanoparticle sample through a metal-coated fiber tip and far-field detection by a collection objective depicted here in transmission mode; (b) simplified 2D model with an aperture tip scanning a nanoparticle sample and flow detectors on the simulation boundaries for transmission (*T*) and reflectivity (*R*).

scanning at constant height will not represent the topography but can minimize the coupling between the optical signal and the topography. To cross-check the influence of height change of the tip, these two different working modes of SNOM are simulated and discussed separately.

Considering all the variables of the tip-matter interaction system, it is important to investigate the influence of each parameter to establish a reliable simulation model. In the following sections, we will study the critical parameters and discuss their influence on the SNOM results to develop a realistic simulation model capable of describing experimental measurement.

2.2. SNOM setup in FEM simulation

Figure 4 depicts the tip-matter system consisting of the aperture probe, the nanoparticle sample, and the far-field detection, all to be considered in the FEM simulation. However, it is impossible for COMSOL to deal with such a complex 3D model. To simplify the simulation, we transform it into a 2D model given in figure 4(b). Regularly arranged silver nanoparticles are placed on a glass substrate. In the middle of the fully considered fiber tip, a plane-wave light

source is introduced propagating along the tip towards the sharp opening. The particles are then illuminated with the localized electric field exciting the aperture.

The tip location is defined based on the vertical (height) and lateral position of the central opening. By controlling the height and position of the tip across the sample can be simulated and the tip-sample gap tuned. Two different modes are studied: For the constant-height mode, the height of the tip is fixed at a constant distance above the glass substrate, which equals the maximum elevation of the sample surface plus the gap value. By using parameter sweeping in COMSOL, the position of the tip opening is varied to simulate the tip scanning across the sample surface. For the constant-gap mode in contrast, we first use a Matlab code to define the scanning path of the tip for a specific sample surface. The tip-surface distance is now fixed to the gap value but the height is changing according to the geometry of the sample surface while the tip is scanned across. We then import the scanning path into the COMSOL model for further simulations.

Transmission and reflectivity are recorded by computing the power flows through the boundaries labeled with *T* and *R*, respectively, while the tip is scanned across the nanoparticle

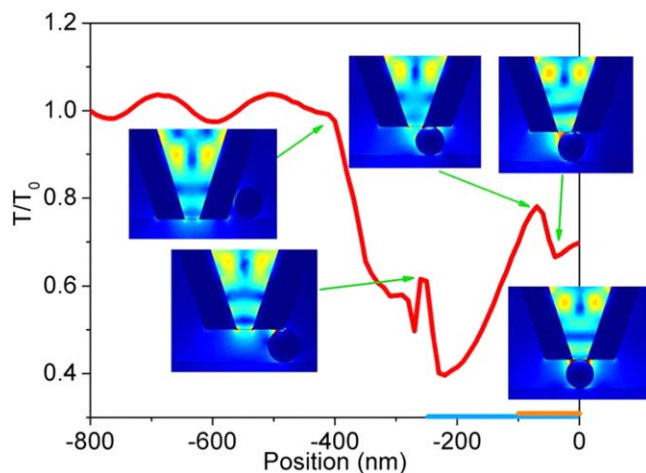


Figure 5. Normalized transmission signal of a basic 2D a-SNOM simulation model with a tip of 100 nm aperture, 200 nm aluminum coating, and 20° cone angle scanning at a constant gap of 1 nm across a single spherical silver nanoparticle of 200 nm diameter on a glass substrate; the insets visualize near-field distributions for the indicated tip positions. On the abscissa, the orange bar represents the radius of the particle, and the blue bar the radius of the end of the tip including opening and coating.

sample. To evaluate the field enhancement, the transmission and reflectivity signals are normalized to the corresponding signals obtained from scanning an area without a nanoparticle.

3. Results and discussion

3.1. Influence of aperture size, coating thickness, and cone angle

Using COMSOL simulation software, the parameters aperture size, coating thickness, and cone angle of the geometry are studied in both modes, constant gap and constant height. The simulations start from the following parameter set with all values fixed at the given numbers except for the specified one being varied: a tip with 100 nm aperture size (opening), 200 nm thick aluminum coating (coating), and 20° cone angle, scanning at 1 nm gap across a single spherical silver nanoparticle of 200 nm diameter on a glass substrate. The silver nanoparticle is centered at position zero whilst the x -axis in the following figures represents the position of the aperture center. The transmitted field distribution is recorded and normalized with a value far away from the particle position (i.e. background without nanoparticle). The simulation result for the transmission signal of the model with the basic parameter set is shown in figure 5. The insets represent the near-fields when the tip is at the specific positions indicated.

Starting far away from the nanoparticle (high negative values on the x -axis), the normalized transmission equals one by definition. When approaching the nanoparticle, an interference-like pattern is visible which could result from the superposition of the partial waves coming directly from the SNOM tip and those scattered from the nanoparticle. At the

moment when the tip reaches the nanoparticle and moves up in constant-gap mode, the signal starts to drop as the particle will absorb the light and screen the transmission. Peaks in that generally lower signal range are found in the cases of strong local field enhancement at the aperture edges when the corresponding scattered light can pass by the nanoparticle. As the tip aperture starts to move directly over the nanoparticle, high local fields are observed in between the tip and nanoparticle, the detection in the far field is however blocked as the corresponding local minimum in the transmission indicates. The dependence of the detailed transmission signal on the different parameters will be investigated in the following.

In general, it is clear that far away from the nanoparticle the signals for constant-height and constant-gap mode are highly similar due to the normalization with the reference case of the respective mode and no near-field information from the nanoparticle being present. Within the particle range, however, i.e. when the tip starts to rise to the height of the particle diameter (plus gap) for constant-gap mode, and the tip edge is on top of the particle for constant-height mode, differences occur. The shape of the transmission signals is still similar for both scanning modes, but for constant-gap scanning the average drop in signal intensity and hence contrast is much larger than for constant-height scanning, due to the change of height between tip and substrate. The cases of constant-height and constant-gap mode are represented on the left and right column of figure 6, respectively. Then, the critical parameters of the tip geometry are studied and the normalized transmission intensity, i.e. the transmission with nanoparticle (T) normalized to the transmission without nanoparticle (T_0) presented.

As the aperture size increases, it is expected that the far-field regime starts to dominate the light-matter interaction. Considering the diffraction limit, it is reasonable to assume that this happens when the aperture becomes larger than $\lambda/2$. Since in the simulation 532 nm is used for the wavelength of the illuminating light, a tip with an aperture of more than 266 nm is expected to prevalently lead to illumination in the far-field regime. When the aperture size increases from 100 to 300 nm as illustrated in figures 6(a) and (b), it is clearly visible that from 260 nm on the transmission signal changes, which is due to the increasing predominance of the far-field suppressing the visibility of near-field information. This is very pronounced in constant-height mode [figure 6(a)] but also happens for constant-gap scanning despite the gap between the tip and the particle remaining at just 1 nm. When illuminating through a sufficiently small aperture in contrast, an enhancement within approximately 50 nm around the particle surface can be obtained as expected from previous work [29]. It is interesting to note that the transmission signal for the 300 nm aperture size also seems to show an enhancement outside the nanoparticle and a drop towards its center with an even higher contrast. Yet, this signal does not represent near-field features but may be seen as a result of geometrical configuration: the peak occurs when the edge of the aperture is right above the center of the nanoparticle. In this case, light exiting the aperture at the side of the nanoparticle could be reflected from it and eventually double-

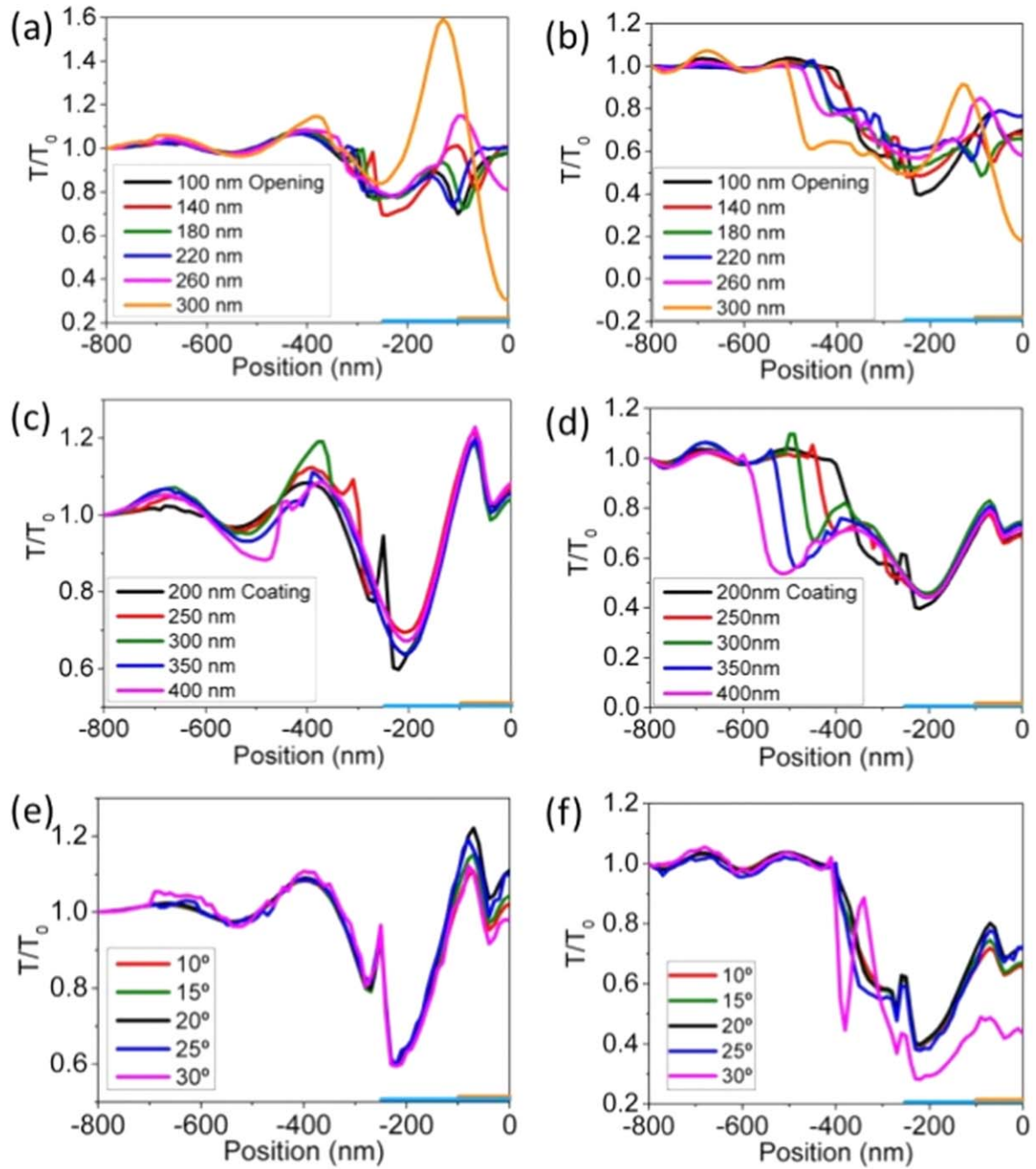


Figure 6. Influence of variable parameters of the tip: (a) and (b) aperture size (opening), (c) and (d) aluminum-coating thickness (coating), and (e) and (f) cone angle; the two different scanning modes, constant height, and constant gap, are represented on the left and right, respectively. If parameters are not varied, they are set to 100 nm opening, 200 nm coating, 20° cone angle, and 1 nm tip-particle distance (gap). On the abscissa, the orange bar represents the radius of the nanoparticle (100 nm), and the blue bar the radius at the end of the tip including opening and coating for the reference case.

reflected from the coating, thus increasing transmission. The subsequent drop of the signal is attributed to the shadowing effect of the nanoparticle which is maximum when the tip is centered above it.

In contrast to the aperture size, varying the coating thickness introduces much less difference for constant-height scanning as shown in figure 6(c). Only the small spike in transmission moves, following the changed position when the tip edge crosses the particle center (−250 nm for 200 nm coating, −300 nm for 250 nm coating, etc). The onset of the

strong decrease in intensity (around −400 nm), however, remains unchanged as the tip stays at the same height. In contrast, for constant-gap mode, the position of this signal minimum shifts according to the diameter of the tip. For thicker coatings, the diameter of the tip end increases and the tip moves downward at a corresponding larger distance from the nanoparticle. This influence of the tip-end diameter on the optical signal is clearly visible in figure 6(d). One observation for both, constant-height and constant-gap mode, is that the fine features start to blur as the coating thickness increases

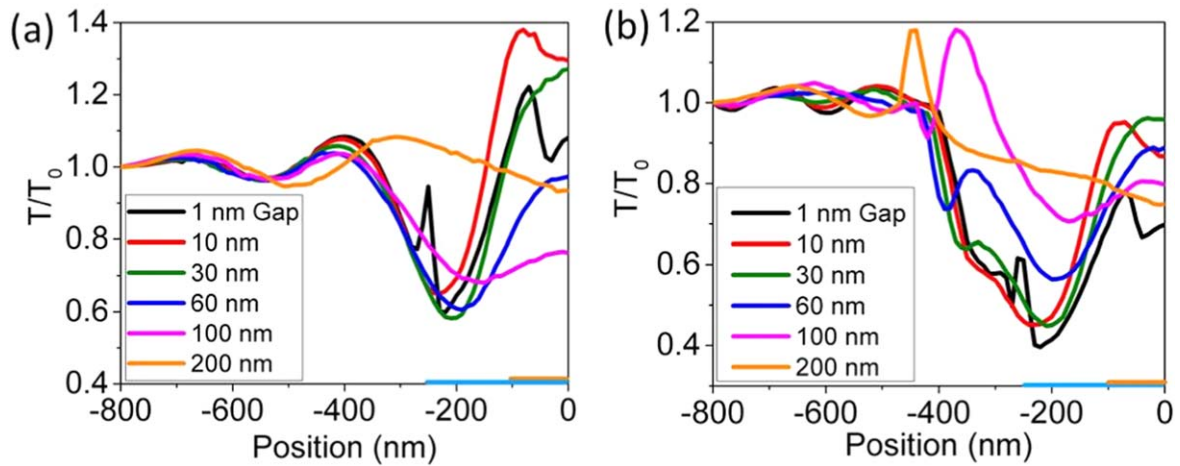


Figure 7. Influence of the tip-particle distance for (a) constant-height and (b) constant-gap scanning mode. On the abscissa, the orange bar represents the radius of the particle, and the blue bar the radius at the end of the tip including opening and coating.

and that for 400 nm thickness, they are only preserved directly at the particle position.

Finally, figures 6(e) and (f) show the influence of changing the cone angle on the normalized transmission signal in constant-height and constant-gap mode, respectively. Overall, there are little changes in the signal shape but a small rise in intensity as long as the aperture is on top of the nanoparticle when the cone angle increases from 10° to 25°. With increasing cone angle, the inner edge of the aperture will become sharper and a stronger near-field is expected to be generated. When the cone angle reaches 30°, however, we observe a drop in transmission signal which is highly pronounced for constant-gap mode. In this latter case, also an additional peak occurs when the tip is moving down, indicating that tip angles above 25° lead to a loss in near-field signal just as the larger openings do since the interaction of the aperture and the nanoparticle is not as localized anymore.

Summarizing the influence of scanning modes and tip geometry parameters, we can say that in comparison with constant-height, constant-gap scanning generates a higher contrast of the transmission signal between the nanoparticle and the background of the substrate (also consider the different scaling on the y-axis). This may originate from the convolution of the optical with the topographic signal. Furthermore, the distance between the tip and the bare substrate is much larger in constant-height scanning, so that part of the scattered light might not reach the detector. However, the tip parameters show similar influence for both, constant-gap and constant-height mode as long as the tip is on top of the nanoparticle. Increasing the aperture size turns near-field into far-field excitation, resulting in a loss of fine features around the particle. Thicker coatings mean a bigger tip-end size, which changes the signal when the tip starts to interact with the nanoparticle but has little influence when the tip is above the particle. The cone angle of the tip just changes the transmission signal slightly except for when it reaches 30°. For large cone angles, the tip moves down more slowly due to the low slope, but at the same time, the distance from the aperture to the nanoparticle increases earlier.

Another central parameter of the tip-matter interacting system is the distance between the tip and the nanoparticle. Figures 7(a) and (b) depict the simulation results for different minimal tip-particle distances (gap) in constant-gap and constant-height scanning mode, respectively. Hereby, the gap corresponds to the smallest distance between the tip and nanoparticle in constant-height mode and to the constant distance to the sample surface in the case of constant gap. In both modes, for gaps up to 10 nm, the drop of transmission intensity at the particle center (zero position) and the enhancement peak at the particle side (within 150 nm) are clearly visible, see the black and red lines. From 30 nm gap on, the valley starts to disappear and so does the peak as the gap further increases to 200 nm. These are clear indications that the near-field information gets lost since the excitation no longer takes place in the near-field regime. At the same time, initially, more of the light exiting the tip can pass the nanoparticle (rise of the signal at the particle position) until again the light becomes scattered out of the detector range (further increase of gap). The peak when the tip edge is closest to the nanoparticle (position -250 nm) disappears in constant-height mode when the gap is larger than a few nm. In constant-gap mode corresponding features remain, yet are shifted farther and broaden. It is clear that the smallest possible gap will provide the highest resolution, and gaps above 10 nm will result in a gradual loss of near-field information.

3.2. Influence of tip shape

Concluding from the simulations of varying aperture size, coating thickness, cone angle, and tip-particle distance, it was identified that the first (called opening) and the last (called gap) parameter have the largest influence on the transmitted intensity. Additionally, the SEM picture in figure 2(d) revealed that the tip end is not smooth but contains protruding structures, which should also be considered in a realistic simulation model for SNOM. Thus, we investigate different tip shapes as depicted in figure 8.

Due to the fabrication method, it is impossible to fabricate a smooth surface at the opening and at the end of the

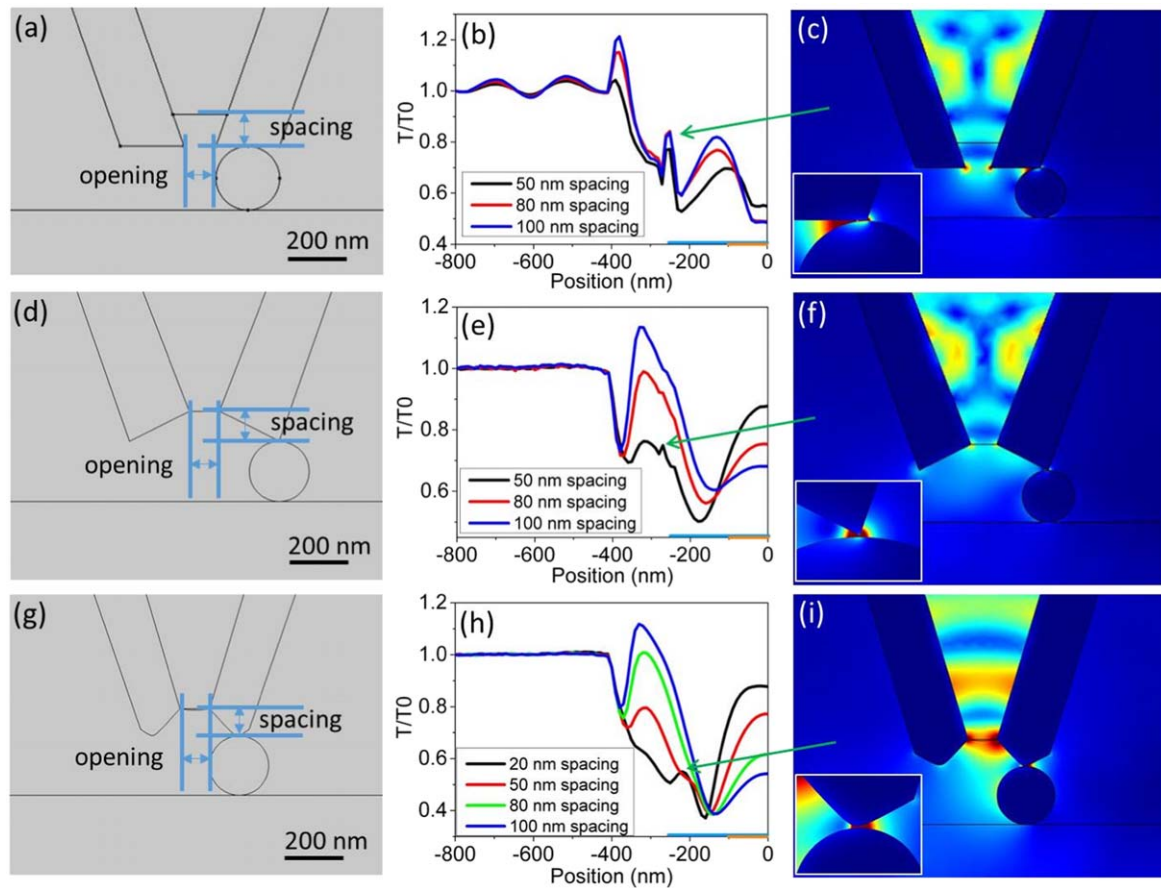


Figure 8. Influence of variable tip shapes in constant-gap scanning mode. (a), (d), and (g) are sketches of the simulated model. Tip opening, coating thickness, and cone angle are 100 nm, 200 nm, and 20° , respectively, and the gap is 1 nm. The particle is made from silver and has a 200 nm diameter. (b), (e), and (h) are the simulation results of normalized transmission intensity as a function of varied spacing as indicated in (a), (d), and (g). Position means the relative distance between the center of the tip and the nanoparticle. On the abscissa, the orange bar represents the radius of the particle, and the blue bar the radius at the end of the tip including opening and coating. (c), (f) and (i) show the normalized electric field distribution for 100 nm spacing revealing the highly localized near-field excitation which is underlined by the zoom-in images highlighting the tip-particle interaction.

coating. In addition, the deposition of aluminum results in a protruding lip at the tip opening [see figure 2(d)]. To understand the influence of the shape on the a-SNOM results, the aperture is assumed to be recessed, beveled, or crater-shaped as shown in figures 8(a), (d), and (g), respectively. For each model, the spacing, i.e., the space between the front end of the coating and the flat end of the glass fiber was varied. In figures 8(b), (e), and (h), respectively, the simulation results of scanning the three types of apertures in constant-gap mode across a single silver nanoparticle with 200 nm diameter are presented. All the simulations are based on the reference model of constant-gap scanning mode with parameters of 100 nm opening, 200 nm coating thickness, 20° cone angle, and 1 nm gap between tip and nanoparticle. Transmission results with nanoparticle (T) are again normalized to transmission results without nanoparticle (T_0) and for simplicity just called ‘transmission’. To highlight the interaction between the tip and the nanoparticle, the normalized electric field distribution for the case where the sharp tip edge is closest to the nanoparticle is exemplarily imaged in figures 8(c), (f), and (i), and linked to the original peaks in the line scans. The spacing is

100 nm, thus the peaks disappear when the field enhancement is highly localized, see below.

In the case of a recessed aperture [figure 8(a)], the shape of the transmission signal looks similar for different spacing values [figure 8(b)]. However, increasing the spacing results in a higher signal contrast. As the spacing is enlarged from 50 to 100 nm, the transmission increases almost along the entire scan except for when the tip is on top of the nanoparticle (position 0); then it drops. Interferences emerge between the fiber end and the tip end that will depend on the spacing (see also the inset in figure 5). If the spacing is such that an intensity maximum occurs at the end of the tip, an overall stronger excitation and thus signal is expected, except for when the tip is directly on top of the nanoparticle. In this case, the transmission is blocked. When the sharp edge at the outer rim of the coating is closest to the nanoparticle, a sharp peak occurs at a position of about -250 nm independent of spacing. The peak does not shift because the diameter of the tip end remains unchanged when varying the spacing. The occurrence of this peak can be correlated to the strong local electric field between tip edge and nanoparticle as depicted in the inset in figure 8(c): a highly confined field enhancement

occurs giving rise to a sharp and well-defined peak. The other two peaks that are visible in the scan can be linked to the situation when the inner rim of the coating shows a strong near-field interaction with the nanoparticle or when the tip has moved side by side with the nanoparticle.

For the beveled aperture [figure 8(d)] the transmission signal looks significantly different. The peak at the position of around -400 nm has changed to a sharp dip followed by a broad peak with a shoulder. The shoulder is a remnant of the sharp peak in figure 8(b) as corroborated by figure 8(f) which details the same relative position between the tip and the nanoparticle as in figure 8(c). Yet, the field enhancement is much more local in particular for larger spacings and hence sharper edges. Therefore, it becomes unlikely to be detected in the far field. Compared to the recessed aperture, the local minimum in transmission when the tip is on top of the nanoparticle (position 0) has changed to a local maximum. In the case of a beveled tip, the enhanced fields emerging between the tip and the nanoparticle can be scattered in the transmission direction which is easier for a smaller spacing when the effective aperture size appears broader than the opening itself. With increasing spacing, which implies steeper and longer terminating walls of the coating, funneling effects may occur that confine the light directly beneath the aperture and hence reduce the transmission signal. An argument for the funneling behavior can be found in the fact that the beveled aperture does not show interferences in the region far away from the nanoparticle (position -800 to -450 nm), which implies that no light becomes scattered from the nanoparticle at this lateral distance. Overall, the beveled aperture appears to be a reasonable shape for the tip when compared to the observations made by SEM [(figure 2(d)). Yet, it would become even more realistic when sharp edges are avoided.

By using a crater-shaped aperture, where a rounded termination of the coating is considered instead of a sloped one, we obtain a simulation model without any sharp edges as shown in figure 8(g). This model comes as close as possible to the SEM image of the aperture probe. As the spacing increases for the crater-shaped aperture, which means that the coating protrudes farther, the transmission signal again becomes smoother, and its contrast increases, just as discussed for the previous tip shape. According to figure 2(d), real apertures still show more details such as noncircular openings or randomly distributed nanograins attached, which are hard to model in a two-dimensional simulation. Regarding the three models presented here, the crater-shaped aperture is the most realistic one and at the same time, the corresponding simulations are stable. Therefore, it was used in the following simulations.

3.3. Comparison with experimental results

Section 2.1 already introduced the experimental results for a-SNOM measurements on regularly arranged silver nanoparticles fabricated by shadow nanosphere lithography. In our experiment, polystyrene spheres with a diameter of 909 nm were used as a mask. Hence the shortest distance between two

neighboring nanoparticles amounts to 525 nm. To study the particle interaction, we simulate a scan of the crater-shaped aperture tip [compare figure 8(g)] across two such silver nanoparticles with a 525 nm distance. The comparison between simulated and experimental results is given in figure 9.

In detail, figures 9(a)–(c) present the experimental result of topography, transmission, and reflectivity obtained from a-SNOM measurements on hexagonally arranged silver nanoparticles. As described in section 2.1, the diameter of these nanoparticles is 140 ± 20 nm. It can clearly be seen that there are two different distances between the silver nanoparticles, from which we chose the shorter amounting to 525 nm. Across a corresponding connection line, marked in green, we extract data from line scans as depicted in figures 9(d)–(f) (also shown in green). The additional red lines present the simulation data for scanning the crater-shaped aperture from figure 8(g) in constant-gap mode across two silver nanoparticles (150 nm in diameter) with 525 nm distance. Both experimental and simulated transmission and reflectivity are normalized to the reference signal without nanoparticles, leading to a so-called normalized enhancement.

When comparing the two datasets, it firstly is visible in topography [see figure 9(d)], that the theoretical tip cannot move fully in between the nanoparticles. So, the contrast appears weaker in the simulation. The reason is that the shape of the real nanoparticles is not a hemisphere but resembles rather a flattened hill. Consequently, the simulated transmission signal is also less pronounced than the experimental counterpart [see figure 9(e)]. The trends, however, are highly comparable with an enhancement occurring at the brink of the nanoparticles or in between them for the shortest distance. However, the slightly elevated transmission signal on top of the nanoparticles as predicted from simulations cannot clearly be identified in the experimental line scan due to the noise. As for the reflectivity [figure 9(f)], the enhancement shows up on top of the particles, both in simulation and experiment. The signal in reflectivity is lower as only part of the back-scattered light is collected by the detector. Furthermore, since the detector needs to be placed asymmetrically in the experiment, which is accordingly considered in the simulation, the peak is not at the exact center of the nanoparticle. The asymmetry is more strongly pronounced in the simulation including one or more shoulder peaks. In the experimental data, the underlying noise prevents a clear identification of such features. Finally, it should not be forgotten that the simulation is set up in 2D for reasons of computational efficiency, and hence variations from the experimental data are to be expected. Nevertheless, experimental and simulated curves are highly comparable and it is confirmed that the normalized reflectivity on top of the nanoparticles is positive, whilst it is negative at the nanoparticle positions in transmission. Altogether, simulations based on a realistic model of a-SNOM are capable of reproducing the major features of the experimental results and can thus also be employed for predicting near-field

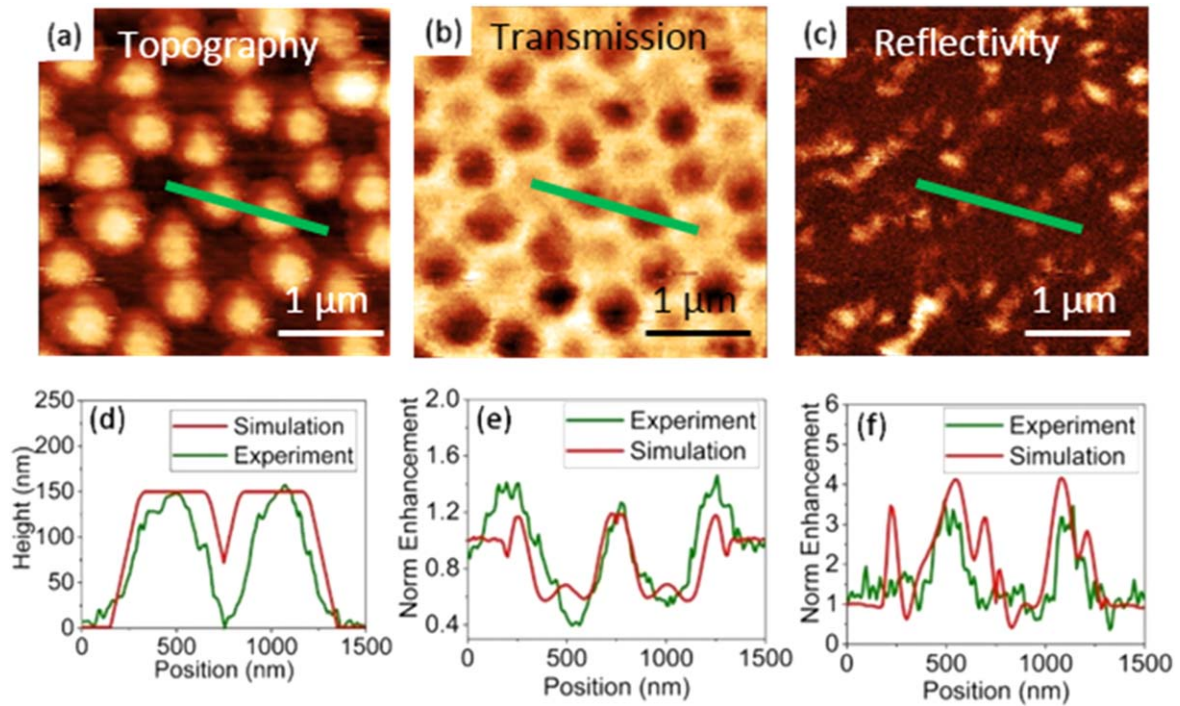


Figure 9. Comparison between experimental and simulated a-SNOM data of Ag nanoparticles. (a), (b), and (c): maps of topography, transmission, and reflectivity, respectively, as measured by a-SNOM. (d), (e), and (f): corresponding experimental (green curve) and simulated (red curve) line scans along the shortest distance between two neighboring nanoparticles. The line along which the experimental data are extracted is marked equally in green in (a)–(c). For the simulation, a constant-gap scan of the crater-shaped aperture across two silver nanoparticles (150 nm in diameter) with a 525 nm distance is assumed. The measurements of transmission and reflectivity are normalized to the background without nanoparticles and the asymmetry in the reflectivity is due to the asymmetric position of the detector as described in the text.

distributions as well as for identifying optimal imaging conditions.

4. Summary

In summary, we developed a multidimensional numerical model based on the finite-element method that provides a realistic description of an a-SNOM measurement. Near-field distributions of regularly arranged silver nanoparticles on a glass substrate were measured by a-SNOM and served as a starting point. To understand the mechanism of tip-nanoparticle interaction, we used the software COMSOL Multiphysics to build up a model for aperture-probe scanning across a nanoparticle. We investigated how the geometry parameters opening size of the aperture, thickness of the aluminum coating, cone angle of the tip, and distance between tip and nanoparticle influence the transmitted light intensity. For variations starting from reasonable parameter values of 100 nm opening, 200 nm coating thickness, 20° cone angle, and 1 nm gap between tip and nanoparticle, we derived that the opening and the gap show the biggest influence. As they increase, near-field information gets lost: the signal contrast seemingly increases, yet the fine features disappear. All these investigations were performed comparatively for constant-height and constant-gap scanning. Considering the shape of the tip, the influence of the protrusion of

the coating at the aperture was investigated and a tip with a crater-shaped coating was determined to provide the most realistic results. By using this final model, we compared the simulation of a line scan across nanoparticles with the corresponding experimental results, both for the signals of transmission and reflectivity, and good agreement was found. The optical model developed can thus support the understanding of image formation in a-SNOM. At the same time, it provides information about adequate parameters to obtain high near-field resolution.

Acknowledgments

Regarding the SNOM setup, the collaboration with all members and technicians of the Fumagalli group from the Freie Universität Berlin is acknowledged. The authors thank Patrick Andrä, Phillip Manley, and Gauri Mangalgi for discussions about simulations. This work was supported by funding from the Helmholtz Association for the Young Investigator group VH-NG-928 within the Initiative and Networking fund. Min Song especially acknowledges the support of funding from the China Scholarship Council. The authors acknowledge support from the Open Access Publication Fund of the University of Duisburg-Essen.

Data availability statement

The data cannot be made publicly available upon publication because they are not available in a format that is sufficiently accessible or reusable by other researchers. The data that support the findings of this study are available upon reasonable request from the authors.

ORCID iDs

M Schmid  <https://orcid.org/0000-0001-5103-0750>

References

- [1] Bozhevolnyi S I and Pudonin F A 1997 Two-dimensional micro-optics of surface plasmons *Phys. Rev. Lett.* **78** 2823–6
- [2] Pohl D W and Courjon D 1993 *Near Field Optics, Kluwer, The Netherlands.*
- [3] Yin L, Vlasko-Vlasov V K, Pearson J, Hiller J M, Hua J, Welp U, Brown D E and Kimball C W 2005 Subwavelength focusing and guiding of surface plasmons *Nano Lett.* **5** 1399–402
- [4] Imura K, Nagahara T and Okamoto H 2005 Near-field optical imaging of plasmon modes in gold nanorods *J. Chem. Phys.* **22** 154701
- [5] Dvořák P, Neuman T, Břínek L, Šamořil T, Kalousek R, Dub P and Šíkola T 2013 Control and near-field detection of surface plasmon interference patterns *Nano Lett.* **13** 2558–63
- [6] Tuniz A, Chemnitz M, Dellith J, Weidlich S and Schmidt M A 2017 Hybrid-mode-assisted long-distance excitation of short-range surface plasmons in a nanotip-enhanced step-index fiber *Nano Lett.* **17** 631–7
- [7] Zayats A V, Smolyaninov I I and Davis C C 1999 Observation of localized plasmonic excitations in thin metal films with near-field second-harmonic microscopy *Opt. Commun.* **169** 93–6
- [8] Futamata M and Bruckbauer A 2001 ATR-SNOM-Raman spectroscopy *Chem. Phys. Lett.* **341** 425
- [9] Murazawa N, Ueno K, Mizeikis V, Juodkazis S and Misawa H 2009 Spatially selective nonlinear photopolymerization induced by the near-field of surface plasmons localized on rectangular gold nanorods *J. Phys. Chem. C* **113** 1147–9
- [10] Tanaka Y Y, Komatsu M, Fujiwara H and Sasaki K 2015 Nanoscale color sorting of surface plasmons in a double-nanogap structure with multipolar plasmon excitation *Nano Lett.* **15** 7086–90
- [11] Kawasaki N, Meuret S, Weil R, Lourenço-Martins H, Stéphane P and Kociak M 2016 Extinction and scattering properties of high-order surface plasmon modes in silver nanoparticles probed by combined spatially resolved electron energy loss spectroscopy and cathodoluminescence *ACS Photon.* **3** 1654–61
- [12] Tománek P, Škarvada P, Macků R and Grmela L 2010 Detection and localization of defects in monocrystalline silicon solar cell *Adv. Opt. Technol.* **2010** 1–5
- [13] Silva T J, Schultz S and Weller D 1994 Scanning near-field optical microscope for the imaging of magnetic domains in optically opaque materials *Appl. Phys. Lett.* **65** 658–60
- [14] Kruk S, Slobozhanyuk A, Denkova D, Poddubny A, Kravchenko I, Miroshnichenko A, Neshev D and Kivshar Y 2017 Edge states and topological phase transitions in chains of dielectric nanoparticles *Small* **13** 1603190
- [15] Herrmann M, Neuberth N, Wissler J, Pérez J, Gradl D and Naber A 2009 Near-field optical study of protein transport kinetics at a single nuclear pore *Nano Lett.* **9** 3330–6
- [16] Abramczyk H, Surmacki J, Kopeć M, Olejnik A K, Kaufman-Szymczyk A and Fabianowska-Majewska K 2016 Epigenetic changes in cancer by Raman imaging, fluorescence imaging, AFM and scanning near-field optical microscopy (SNOM). Acetylation in normal and human cancer breast cells MCF10A, MCF7 and MDA-MB-231 *Analyst* **141** 5646–58
- [17] Girard C and Dereux A 1996 Near-field optics theories *Prog. Phys.* **59** 657
- [18] Greffet J J and Carminati R 1997 Image formation in near-field optics *Prog. Surf. Sci.* **56** 133–237
- [19] Rotenberg N and Kuipers L 2014 Mapping nanoscale light fields *Nat. Photon.* **8** 919–26
- [20] Minovich A, Klein A E, Janunts N, Pertsch T, Neshev D N and Kivshar Y S 2011 Generation and near-field imaging of airy surface plasmons *Phys. Rev. Lett.* **107** 116802
- [21] Mote R G, Yu S F, Kumar A, Zhou W and Li X F 2011 Experimental demonstration of near-field focusing of a phase micro-Fresnel zone plate (FZP) under linearly polarized illumination *Appl. Phys. B* **102** 95–100
- [22] Schmid M, Grandidier J and Atwater H A 2013 Scanning near-field optical microscopy on dense random assemblies of metal nanoparticles *J. Opt.* **15** 125001
- [23] Mihaljevic J, Hafner C and Meixner A J 2013 Simulation of a metallic SNOM tip illuminated by a parabolic mirror *Opt. Express* **21** 25926–43
- [24] Semenenko V, Liu M and Perebeinos V 2022 Simulation of scanning near-field optical microscopy spectra of 1D plasmonic graphene junctions *Opt. Express* **30** 9000–7
- [25] Dvorak P *et al* 2017 Imaging of near-field interference patterns by aperture-type SNOM—influence of illumination wavelength and polarization state *Opt. Express* **25** 16560–73
- [26] Denkova D, Verellen N, Silhanek A V, Valev V K, Van Dorpe P and Mashchakov V V 2013 Mapping magnetic near-field distributions of plasmonic nanoantennas *ACS Nano* **7** 3168–76
- [27] Abbasirad N, Barreda A, Chen Y-J, Huang J-S, Staude I, Setzpfandt F and Pertsch T 2022 Near-field launching and mapping unidirectional surface plasmon polaritons using an automated dual-tip scanning near-field optical microscope *Photon. Res.* **10** 2628–41
- [28] Kosiorek A, Kandulski W, Chudzinski P, Kempa K and Giersig M 2004 Shadow nanosphere lithography: simulation and experiment *Nano Lett.* **4** 1359–63
- [29] Schmid M, Andrae P and Manley P 2014 Plasmonic and photonic scattering and near fields of nanoparticles *Nanoscale Res. Lett.* **9** 1–11